Organic Electronics 17 (2015) 138–143

Contents lists available at ScienceDirect

Organic Electronics

journal homepage: www.elsevier.com/locate/orgel

Thickness dependent barrier performance of permeation barriers made from atomic layer deposited alumina for organic devices

Hannes Klumbies [a], Peter Schmidt [a], Markus Hähnel [a], Aarti Singh [b], Uwe Schroeder [b], Claudia Richter [b], Thomas Mikolajick [b,c], Christoph Hoßbach [c], Matthias Albert [c], Johann W. Bartha [c], Karl Leo [a], Lars Müller-Meskamp [a,*]

[a] Institut für Angewandte Photophysik, Technische Universität Dresden, George-Bähr-Str. 1, 01062 Dresden, Germany
[b] Nanoelectronics Materials Laboratory NaMLab gGmbH, Noetznitzer Str. 64, 01187 Dresden, Germany
[c] Institute of Semiconductor and Microsystems, Technische Universität Dresden, Nöthnitzer Str. 64, 01062 Dresden, Germany

ARTICLE INFO

Article history:
Received 10 September 2014
Received in revised form 1 December 2014
Accepted 2 December 2014
Available online 12 December 2014

Keywords:
ALD
Defect density
Thickness dependency
Electrodeposition
WVTR
OLED

ABSTRACT

Organic devices like organic light emitting diodes (OLEDs) or organic solar cells degrade fast when exposed to ambient air. Hence, thin-films acting as permeation barriers are needed for their protection. Atomic layer deposition (ALD) is known to be one of the best technologies to reach barriers with a low defect density at gentle process conditions. As well, ALD is reported to be one of the thinnest barrier layers, with a critical thickness – defining a continuous barrier film – as low as 5–10 nm for ALD processed Al_2O_3. In this work, we investigate the barrier performance of Al_2O_3 films processed by ALD at 80 °C with trimethylaluminum and ozone as precursors. The coverage of defects in such films is investigated on a 5 nm thick Al_2O_3 film, i.e. below the critical thickness, on calcium using atomic force microscopy (AFM). We find for this sub-critical thickness regime that all spots giving raise to water ingress on the $20 \times 20\ \mu m^2$ scan range are positioned on nearly flat surface sites without the presence of particles or large substrate features. Hence below the critical thickness, ALD leaves open or at least weakly covered spots even on feature-free surface sites. The thickness dependent performance of these barrier films is investigated for thicknesses ranging from 15 to 100 nm, i.e. above the assumed critical film thickness of this system. To measure the barrier performance, electrical calcium corrosion tests are used in order to measure the water vapor transmission rate (WVTR), electrodeposition is used in order to decorate and count defects, and dark spot growth on OLEDs is used in order to confirm the results for real devices. For 15–25 nm barrier thickness, we observe an exponential decrease in defect density with barrier thickness which explains the likewise observed exponential decrease in WVTR and OLED degradation rate. Above 25 nm, a further increase in barrier thickness leads to a further exponential decrease in defect density, but an only sub-exponential decrease in WVTR and OLED degradation rate. In conclusion, the performance of the thin Al_2O_3 permeation barrier is dominated by its defect density. This defect density is reduced exponentially with increasing barrier thickness for alumina thicknesses of up to at least 25 nm.

* Corresponding author. Tel.: +49 351 46333504.
E-mail address: lars.mueller-meskamp@iapp.de (L. Müller-Meskamp).

http://dx.doi.org/10.1016/j.orgel.2014.12.003
1566-1199/

1. Introduction

Organic solar cells and organic light emitting diodes (OLEDs) are growing technological fields allowing a multitude of new applications [1–3]. While their intrinsic stability is remarkable [4,5], they degrade fast when exposed to water vapor and oxygen [6,7]. Hence, an encapsulation is required for realistic commercial products. Bulk glass represents an excellent encapsulation, but it is heavy, brittle, and non-flexible. As a consequence, inorganic barrier films coated on polymer webs or directly onto the device (thin-film encapsulation) are typically applied as permeation barriers. Contrary to bulk glass, the thin-film encapsulation layers contain defects which represent the dominant path of permeation – permeation through glass or intact barrier material is usually lower by several orders of magnitude [8]. The usual defect density reported for thin-film barriers is in the order of 10,000 cm^{-2} or more [7]. However, defect densities as low as 6000 cm^{-2} with evaporated Al [9] or even 500 cm^{-2} with PECVD processed Si_3N_4 [10] have been reported. Atomic layer deposition (ALD) is often claimed to allow defect-free layers [7], which would be ideal for barriers. However, this turns out to not be true under all conditions – especially for low-temperature deposition required for processing on organic devices. To reveal the defects in a 25 nm thick Al_2O_3 layer grown by ALD at 120 °C, Zhang et al. [11] used electrodeposition of copper to decorate pinholes. They found the defect density to depend on the substrate: A defect density as low as 38 cm^{-2} was detected on a nickel-covered silicon wafer, while the use of a rougher copper-substrate leads to significantly higher defect densities. On a polished copper surface deposited on a silicon wafer, Abdulagatov et al. [12] found only 8 defects per cm^2. Dameron et al. [13] and Langereis et al. [14] stressed that the cleanliness of the substrate plays a crucial role toward a low defect density. For barrier layers in general, several authors [10,14,15] found a sudden increase in barrier performance over orders of magnitude when reaching the so called "critical thickness" of their process. The general understanding of this increase in barrier performance is that the deposited material forms a continuous layer at this thickness, i.e. the residual defects in the layer and not the substrate material limit the permeation. For ALD processed Al_2O_3, a critical thickness between 5 and 10 nm was found: Groner et al. [15] looked at low thicknesses and observed a critical thickness of around 5 nm for continuous film formation and a further strong decrease of the WVTR until a saturation thickness of 10 nm when depositing the Al_2O_3 on polyethylene naphthalate (PEN) at 120 °C. Langereis et al. [14] also observed a strong drop in barrier performance below 10 nm followed by a WVTR saturation around 20 nm for a plasma assisted room temperature deposited alumina on PEN. The dependence of the WVTR on the ALD alumina layer thickness was further investigated by Carcia et al. [16,17], who presented an exponential improvement in water vapor transmission rate (WVTR) between 5 and 10 nm with increasing layer thickness as it is reported in this paper for thicker layers. They further showed that processing at higher temperatures is an alternative to reach lower WVTRs. For low temperature ALD, Singh et al. [18] showed that not only the sheer number of process cycles but also the ozone pulse duration defines the number of residual defects in the barrier.

In this work, we investigate defects present in the sub-critical thickness regime by using atomic force microscopy (AFM). Thereafter, we conduct a systematical study of how different aspects of barrier performance (defect density, WVTR, and device degradation) are influenced by the Al_2O_3 thickness, i.e. the number of ALD cycles. For each of the thicknesses of 15, 20, 25, 50, and 100 nm Al_2O_3, we use three different sample types.

Like Zhang et al. [11] and Abdulagatov et al. [12], we deposit ALD layers on a copper surface – our first sample type – and use electrodeposition to decorate defects with large copper bumps allowing us to count the defects directly. Since defects of different size differ in their contribution to the barrier performance [9,10], the defect density alone does not give full information about the barrier quality.

As our second sample type, we use calcium thin-films to conduct electrical calcium corrosion tests [19–21] and measure the WVTR as an integral measure of barrier quality.

Our third sample type for Al_2O_3 thin-films is a complete OLED on glass. It is used to confirm the thickness influence for real devices: While the devices used here can be treated as intrinsically stable for the means of this experiment [22], these devices are highly sensitive against moisture entering the device through defects in the aluminum top electrode [9,23] when exposed to air. As a consequence, a circular area around these defects turns inactive (dark spot) and grows over time of air exposure. Note that the Al represents a barrier on its own. Hence for this sample type, the Al_2O_3 thin-films have to cover the holes left in the Al top electrode only and thereby reduce dark spot formation instead of producing a continuous layer on its own.

2. Materials and methods

All substrates used in this work (glass, 25 × 25 mm^2) were cleaned in N-methyl-2-pyrrolidone (20 min), deionized water (10 min), and ethanol (10 min) prior to being dried using a spin-rinser. After cleaning, thermal evaporation was used to cover the glass substrates with either 100 nm Cu layers, or calcium test structures, or OLED devices. For thermal evaporation, transport, storage, and atomic layer deposition, the samples were kept in inert gas atmosphere (N_2) to avoid degradation. Thus, their first air contact was at the beginning of the sample evaluation, i.e. defect decoration, Ca-test, and OLED degradation, respectively.

The ALD was carried out using a hot wall reactor (TFS 500, Beneq Oy) in a clean room class 100 area. As precursors, TMA (trimethylaluminum, semiconductor grade, Air Products GmbH) and ozone (from 99.9995% pure oxygen with ozone generator OP-250P-T1, TMEIC) were used. The Al_2O_3 layers of the thickness series had a thickness of 15, 20, 25, 50, and 100 nm. The applied ALD process

resulted in a growth of ca. 0.1 nm per cycle using a deposition temperature of 80 °C and pulsing times of 0.35 s TMA, 1 s purging, 15 s ozone, and 10 s purging. Throughout the deposition, the nitrogen purging gasflow was 300 sccm. For optimal comparison, all sample types (Cu layers from electrodeposition, Ca-test structures, and OLEDs) were coated in parallel in the very same ALD runs, i.e. there was only one ALD-run per thickness.

For the topography scans, a cleaned glass substrate was covered on full area with 60 nm Ca by thermal evaporation and 5 nm Al_2O_3 by ALD (thickness confirmed by XRR-measurement on silicon reference samples). After ALD processing, the sample was investigated at ambient atmosphere over 48 h by means of consecutive AFM-scans (Dimension 3100 Atomic Force Microscope, VEECO) in tapping mode.

On the copper samples, electrodeposition was used after ALD to render the defects in the Al_2O_3 thin-films visible. After barrier deposition, those samples were put into a copper sulfate bath (CUBRAC 600, Coventya GmbH) for 15 min while a voltage applied between the sample (cathode with ca. 5 cm^2 surface area) and the anode (copper phosphorous alloy with ca. 5 cm^2 surface area) placed in a distance of ca. 4 cm from the sample. The voltage between sample and anode was controlled to provide a constant value of −0.3 V (optimized in a series of cyclic voltammetry experiments) between the sample and an additional Ag/AgCl reference electrode (Sensortechnik Meinsberg GmbH) which was placed close to the sample surface via a Haber–Luggin capillary. Afterward, images of the samples were taken (PowerShot G9, Canon) allowing to identify copper bumps of at least 30 μm diameter. Note that the corresponding defects are much smaller than 30 μm.

Calcium test structures were used to measure the WVTR. While for calcium test evaluation, a homogeneous top to bottom corrosion of the calcium film is assumed, correct WVTRs are also measured for inhomogeneous corrosion caused by the pinhole pattern in the barrier [21,24]. Details of the applied test design were described by Schubert et al. [20]. In the present work, the calcium thickness was 60 nm and the Al-electrode had a thickness of 100 nm. In addition, we added a 100 nm thick protective C_{60}-coating directly on top of the calcium structures in order to avoid damages of the barrier caused by interaction with calcium or corroding calcium [25]. For these experiments, two separate samples were used per thickness; in the case of 50 nm, five samples were used.

The OLED devices used in this work use a similar stack as the one described by Meerheim et al. [22]. For the OLEDs, indium tin oxide (ITO) covered glass substrates were used and the stack of 160 nm organic material was covered by a 100 nm thick Al top electrode. In detail, the stack of organic material consists of a 60 nm thick hole-transporting layer of MeO-TPD (N,N,N′,N′-tetrakis(4-methoxyphenyl)-benzidine) p-doped with 4 wt% F6TCNNQ (2,2′-(perfluoronaphthalene-2,6-diylidene)dimalononitrile), a 10 nm thick electron blocking layer of α-NPD (N,N′-Di(naphthalen-1-yl)-N,N′-diphenyl-benzidine), a 20 nm thick emitter layer consisting of α-NPD with 10 wt% of the red emitter molecule $Ir(MDQ)_2(acac)$ (iridium(III)bis(2-methyldibenzo-[f,h]chinoxalin)(acetylacetonat)) followed by a 10 nm thick hole blocking layer of $BAlq_2$ (aluminum(III)bis(2-methyl-8-quninolinato)-4-phenylphenolate), a 60 nm thick electron transport layer of BPhen (bathophenanthroline; 4,7-diphenyl-1,10-phenanthroline) and Cesium in the ratio 1:1. After the ALD process, the OLEDs were stored at 38 °C and an ambient humidity of 15–20% rh for 45 days with no voltage applied. For intermediate degradation monitoring, the OLEDs were temporarily removed from the aging box several times. During the characterization, a voltage of 5 V was applied and images of each single pixel were captured (MikroCam 5.0MP, Bresser) under a light microscope (Labophot 2, 3.2× magnification, Nikon). The images were evaluated with respect to their inactive area (dark spots area), while degradation from the pixel edges (corners of cover electrode) was excluded from the evaluation. In these experiments, 8 separate OLED-pixels (6.25 mm^2 each) were evaluated per Al_2O_3 thickness.

3. Results and discussion

Surface roughness and particles are often reported to cause defects, i.e. sites of relevant water ingress, in ALD layers [11–14]. Prior to investigating how the thickness of ALD layers affects the barrier defect density, we used atomic force microscopy (AFM) to get a better understanding of the density and shape of the defects in the sub-critical thickness regime. Fig. 1 shows two AFM scans carried out on a calcium film protected by 5 nm Al_2O_3 (ALD). Both scans show the same sample position before and after 48 h of exposure to ambient conditions. Calcium expansion renders the defects visible as water reaching the calcium through defects corrodes the metallic calcium to the more voluminous calcium hydroxide resulting in localized bumps visible in the AFM scans [21].

In the initial AFM scan, numerous pits are visible. Their depth is roughly 7 nm in relation to the smooth surface constituting the rest of the area. The most eye-catching result is that all defects – visible in AFM as localized bumps – have their origin at such surface pits. The noteworthy aspect is that these topography features being related to defects are small and flat and there is no hint for particles being involved in their formation. No pile-up of particles at the borders of the scan area after AFM measurement was visible. Thus, these AFM scans indicate that most of the defects in the sub-critical thickness regime of the ALD are caused by a poor film formation of the regular, i.e. smooth and particle-free, substrate surface. This observation fits very well with the poor barrier performance for films below 5 nm, observed by Groner et al. [15].

The reason for the ALD surface pits is not yet clear. They may originate from height or other irregularities in the calcium film or may be caused during the ALD growth, resulting in a modification of the Ca layer or the ALD layer itself. The latter could for example be caused by residual CH_3 groups from the TMA precursor, that may stick to the calcium stronger than to the Al, which has been reported for silicon substrates [26]. Also molecular surface contamination that sticks during the ALD process but diffuses to form islands might influence the ALD growth negatively. Any of these mechanisms would probably either delay the ALD growth, causing a thinner or less dense layer at these sites

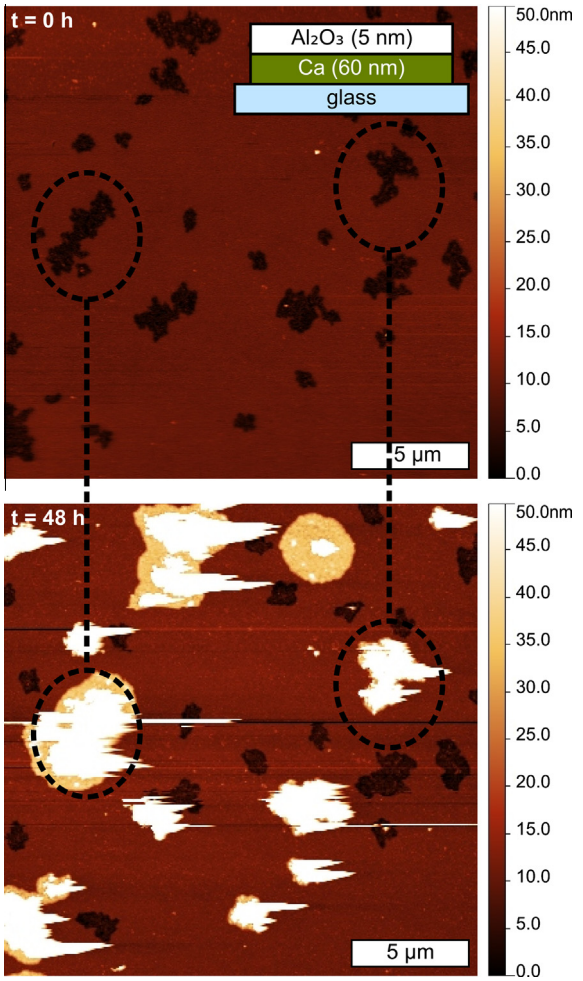

Fig. 1. Defect sites on microscopic scale. Two AFM-scans showing the same area of an Al_2O_3 (ALD) barrier on calcium; one before and one after 48 h under ambient conditions. The inset sketch shows the stack materials of the sample. Bumps in the lower image (volume expansion from oxidized calcium due to water ingress) indicate defect sites in the Al_2O_3 layer. All defects are found at former pit sites. Base plane height and height range were chosen equal for both images for better comparison.

visible as pits, or would cause a topographical weakness to the layer at the step edges and might in turn cause local condensation of water from the ambient atmosphere. Any of these mechanisms would make the barrier more prone to water breakthrough and explain the fast barrier failures at some of these pits. The lateral extent of the pits as well as their distance to each other is in the order of micrometers, i.e. very large compared to the dimensions of single reaction sites. While the origin of the pits remains unclear, we expect them to be characteristic for the sub-critical thickness regime as they are characterized by the absence of large particles or surface features known to define the barrier performance at higher thicknesses.

In the following paragraphs, the results of the defect and WVTR investigations of the Al_2O_3 (ALD) thickness series with 15, 20, 25, 50, and 100 nm thick layers are presented and discussed. The defect densities according to defect decoration using electrodeposition for the 15–100 nm thick ALD layers are shown in Fig. 2. Between 15 and 100 nm of Al_2O_3 thickness the defect density decreases exponentially (a factor of 2 for every 23 nm). From the data, even 15 nm of Al_2O_3 (ALD) form a continuous barrier film with a defect density being far below the defect densities reported for other methods (500–10,000 cm^{-2} or even more [7,10]), but in the same order of magnitude reported for 25 nm thick ALD Al_2O_3 films on a nickel-covered silicon wafer (38 and 59 cm^{-2}) [11]. As the defect density characterization was done at films above 15 nm thickness, the films are past any critical thickness for continuous film formation. In the higher film thickness range of our investigation, no saturation of defect reduction with thickness is observed in the defect density data.

In order to evaluate the integral barrier performance in terms of WVTRs, the same Al_2O_3 thickness series was deposited onto C_{60}-covered calcium-test samples as well. The WVTRs of the 15–100 nm thick Al_2O_3 ALD films measured at 38 °C and ambient humidity (15–20% relative humidity) are shown in Fig. 3 in a semi-logarithmic plot. In the range between 15 and 25 nm, the WVTR decreased roughly exponential with the Al_2O_3 thickness. However above 25 nm, further increase in Al_2O_3 thickness resulted in a sub-exponential (less than exponential) decrease of the WVTR. Along the curve, the scattering of data points decreased strongly with increasing Al_2O_3 thickness. Groner et al. [15] found a well comparable WVTR (ca. 1×10^{-3} g m^{-2} d^{-1}) as we did (ca. 3×10^{-3} g m^{-2} d^{-1}) for a 26 nm thick Al_2O_3 layer. When taking the different climate conditions for measurement into account (the absolute humidity found in 20 °C and 100% rh is the same as in 38 °C and 35% rh), these two values are even equal within experimental limits. However, their WVTR did not drop between 10 and 26 nm and is expected to remain on this level even for higher thicknesses while our WVTR further decreases. Due to this further decrease, one may interpret our data in a way that we have an extraordinary high critical thickness between 25 and 50 nm, but the measured WVTRs of less than 1×10^{-3} g m^{-2} d^{-1} speak in

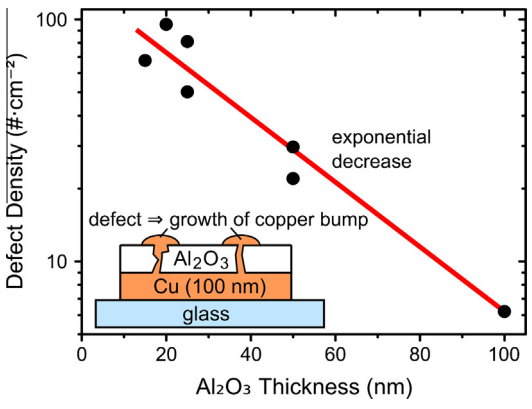

Fig. 2. Defect densities in the Al_2O_3 (ALD) layer thickness series. Defects in the Al_2O_3 (ALD) thin-films of different thicknesses were rendered visible by the electrodeposition of copper into these defects. The continuous line (as a visual guide) highlights the exponential decrease in defect density with increasing Al_2O_3 thickness. The inset sketch shows the schematic cross-section of the sample.

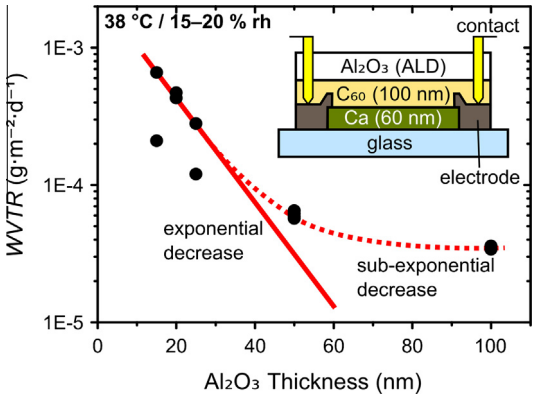

Fig. 3. WVTR values of the ALD Al_2O_3 thin-film barrier series as a function of film thickness measured with electrical calcium corrosion tests. The continuous line (as a visual guide) highlights the exponential decrease in WVTR with increasing Al_2O_3 thickness for lower thicknesses. The inset sketch shows the schematic cross section of the sample.

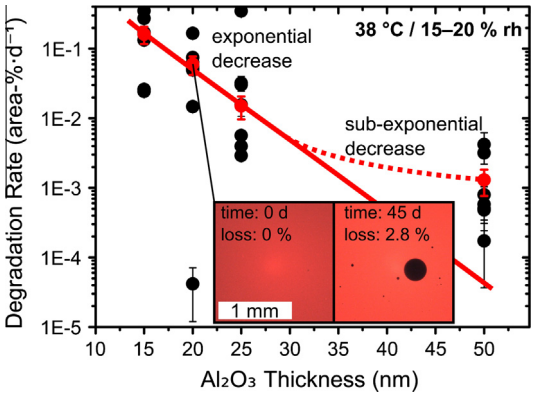

Fig. 4. OLEDs protected by the Al_2O_3 (ALD) barrier thickness series. The loss of active OLED area is shown for each single OLED pixel (black) and as an average (red) of the 8 OLED pixels investigated per Al_2O_3 thickness. The inset illustrates dark spot development on camera images as it was used to obtain the data for this graph. (For interpretation of the references to color in this figure legend, the reader is referred to the web version of this article.)

favor of a continuous film formation (=critical thickness) *below* 15 nm. We, thus, assume that the WVTR was always defined by single defects within the continuous alumina film. Their number decreased with increasing layer thickness. The transition from an exponential to a sub-exponential regime may be a consequence of different types of defects: a large number of comparable defects being covered exponentially with layer thickness that dominates below 25–50 nm and a small number of defects being highly resistant against closure or being formed after the ALD process that stops the exponential decrease in WVTR. In contrast to our work, Groner et al. [15] and Langereis et al. [14] deposited the alumina on polymer films instead of C60-covered glass substrates. Hence, they presumably faced more defects we assume to be highly resistant against closure (like scratches) or to be caused afterward (like covered particles falling off) explaining the absence of an exponentially decreasing WVTR in their data.

OLED devices were the third type of samples investigated in this Al_2O_3 (ALD) barrier thickness series. In contrast to the Cu and Ca-test samples, the complete OLED devices have an aluminum top electrode which already represents a permeation barrier itself. Thus, Al_2O_3 (ALD) thin-film is only required to cover the defects in the aluminum. The quality of this sequential barrier (Al_2O_3 on Al) measured in terms of an active area degradation rate over 45 days of aging is shown in Fig. 4. Between 15 and 25 nm of Al_2O_3 thickness, the degradation rate decreased exponentially with film thickness. Above 25 nm, the observed barrier improvement for thicker Al_2O_3 layers was sub-exponential indicating that the type of dominating defects changed. The deposition of 100 nm Al_2O_3 resulted in large cracks through the Al_2O_3 as well as the aluminum below – maybe originating from differences in thermal expansion coefficients of Al and Al_2O_3 – and lead to a fast degradation of the OLEDs. Therefore, no results are shown for 100 nm thick layers.

On all three types of samples – Cu samples, Ca-test samples, and OLEDs – the different measurement techniques show good correlation. The barrier failure (defect density, WVTR, and degradation) decreased exponentially with the Al_2O_3 thickness for thicknesses in the range of 15–25 nm. This decrease always went along with a decrease in data scattering. For OLEDs and Ca-test samples, barriers thicker than 25 nm still improve with increasing Al_2O_3 thickness, but in a sub-exponential manner.

The dependence between barrier performance and Al_2O_3 thickness was comparable for all three types of samples. Hence, it is reasonable to assume that the growth mechanism on the different samples and, thus, the mechanism of barrier improvement upon thickness increase of the Al_2O_3 layer was similar. The high barrier performances seen in our data speak in favor of continuous alumina films. We, thus, attribute water ingress mainly to a defect driven mechanism, not to bulk diffusion. Hence, we interpret the barrier improvement for thicker Al_2O_3 layers as a reduction and reinforcement of defect sites. While we primarily understand defects as holes, they may also be sites of reduced Al_2O_3 thickness (inhibited growth) prone to corrosion [13,17] and a consequent water breakthrough. The saturation of the exponential decrease for WVTR and OLED degradation upon Al_2O_3 thickness increase for the higher thickness range indicates a number of defects which are more difficult to be covered than the majority of the defects present at 15 nm. These defects could be small scratches, particles falling off after deposition, or defects being caused by the further handling of the samples. Interestingly, the existence of a sub-exponential regime is not found for the copper samples but for samples covered with small molecules like C60; maybe small molecule deposition in particular causes the aforementioned defects. Unfortunately, we can only reason about the origin of these residual defects as we did not find such objects in our AFM scan area of only 6×10^{-6} cm^2. However, we do observe in our AFM-scans that in a sub-critical thickness layer most defects are *not* caused by particles or large surface features. Hence, for producing appropriate permeation barriers with Al_2O_3 (ALD), smooth surfaces and clean room conditions are important to reduce the density of defects that are difficult to cover. The number of ALD cycles required to reach

this bottom line, however, depends on process parameters like temperature, precursor dose, and surface preparation.

4. Conclusions

We investigated Al_2O_3 layers grown by ALD as thin-film permeation barriers for organic device encapsulation in order to get a better understanding of how the barrier layer thickness influences the barrier performance. Investigating Al_2O_3 films of sub-critical thickness via AFM, we observed a high density of defect sites in areas free of large surface features or particles. With a thickness series ranging from 15 to 100 nm Al_2O_3 (ALD) – well above the critical thickness – we were able to show that three different techniques to measure the barrier performance (defect density, WVTR, and ability to protect an OLED device) on three different types of samples all show an exponential improvement with barrier thickness up to 25 nm. Hence, we conclude that the decrease of WVTR and OLED degradation rate with Al_2O_3 barrier thickness is caused by a reduction in defect density as we observed it using electrodeposition. In conclusion, we have demonstrated the importance of optimizing ALD growth parameters like temperature, precursor dose, as well as cleanliness, and the potential of ALD to deposit ultra-high permeation barriers at low thicknesses with highly reproducible quality for the thin-film encapsulation of organic electronic devices.

Acknowledgements

The authors would like to thank the Bundesministerium für Bildung und Forschung in the framework of the Inno-Profile project (03IP602) and the Bundesministerium für Wirtschaft for funding of the AIF project 17131BR. Further thanks are addressed to Waldfried Plieth and Matthias Graf for discussion of the electroplating processes, Harm Knoops for discussions about the surface pits on calcium, to Coventya GmbH for providing the electroplating bath as well as to Sven Kunze, Andreas Wendel (IAPP, TU Dresden), and Dominik Martin (Namlab) for technical assistance and sample preparation.

References

[1] S.R. Forrest, Active optoelectronics using thin-film organic semiconductors, IEEE J. Sel. Top. Quantum Electron. 6 (2000) 1072–1083, http://dx.doi.org/10.1109/2944.902156.
[2] S. Reineke, F. Lindner, G. Schwartz, N. Seidler, K. Walzer, B. Lüssem, et al., White organic light-emitting diodes with fluorescent tube efficiency, Nature 459 (2009) 234–238, http://dx.doi.org/10.1038/nature08003.
[3] M. Riede, T. Mueller, W. Tress, R. Schueppel, K. Leo, Small-molecule solar cells-status and perspectives, Nanotechnology 19 (2008) 424001, http://dx.doi.org/10.1088/0957-4484/19/42/424001.
[4] R. Meerheim, B. Lüssem, K. Leo, Efficiency and stability of p–i–n type organic light emitting diodes for display and lighting applications, Proc. IEEE 97 (2009) 1606–1626, http://dx.doi.org/10.1109/JPROC.2009.2022418.
[5] M. Jørgensen, K. Norrman, S.A. Gevorgyan, T. Tromholt, B. Andreasen, F.C. Krebs, Stability of polymer solar cells, Adv. Mater. 24 (2012) 580–612, http://dx.doi.org/10.1002/adma.201104187.
[6] M. Jørgensen, K. Norrman, F.C. Krebs, Stability/degradation of polymer solar cells, Sol. Energy Mater. Sol. Cells 92 (2008) 686–714, http://dx.doi.org/10.1016/j.solmat.2008.01.005.
[7] J.-S. Park, H. Chae, H.K. Chung, S.I. Lee, Thin film encapsulation for flexible AM-OLED: a review, Semicond. Sci. Technol. 26 (2011) 034001, http://dx.doi.org/10.1088/0268-1242/26/3/034001.
[8] L. Müller-Meskamp, J. Fahlteich, F.C. Krebs, Barrier technology and applications, in: F. Krebs (Ed.), Stab. Degrad. Org. Polym. Sol. Cells, first ed., John Wiley & Sons, Ltd, 2012, pp. 269–329.
[9] H. Klumbies, M. Karl, M. Hermenau, R. Rösch, M. Seeland, H. Hoppe, et al., Water ingress into and climate dependent lifetime of organic photovoltaic cells investigated by calcium corrosion tests, Sol. Energy Mater. Sol. Cells 120 (2014) 685–690, http://dx.doi.org/10.1016/j.solmat.2013.10.023.
[10] A.S. da Silva Sobrinho, G. Czeremuszkin, M. Latrèche, M.R. Wertheimer, Defect-permeation correlation for ultrathin transparent barrier coatings on polymers, J. Vac. Sci. Technol., A 18 (2000) 149–157, http://dx.doi.org/10.1116/1.582156.
[11] Y. Zhang, J.A. Bertrand, R. Yang, S.M. George, Y.C. Lee, Electroplating to visualize defects in Al_2O_3 thin films grown using atomic layer deposition, Thin Solid Films 517 (2009) 3269–3272, http://dx.doi.org/10.1016/j.tsf.2008.12.052.
[12] A.I. Abdulagatov, Y. Yan, J.R. Cooper, Y. Zhang, Z.M. Gibbs, A.S. Cavanagh, et al., Al_2O_3 and TiO_2 atomic layer deposition on copper for water corrosion resistance, ACS Appl. Mater. Interfaces 3 (2011) 4593–4601, http://dx.doi.org/10.1021/am2009579.
[13] A.A. Dameron, S.D. Davidson, B.B. Burton, P.F. Carcia, R.S. Mclean, S.M. George, Gas diffusion barriers on polymers using multilayers fabricated by Al_2O_3 and rapid SiO_2 atomic layer deposition, J. Phys. Chem. C (2008) 4573–4580, http://dx.doi.org/10.1021/jp076866+.
[14] E. Langereis, M. Creatore, S.B.S. Heil, M.C.M. van de Sanden, W.M.M. Kessels, Plasma-assisted atomic layer deposition of Al_2O_3 moisture permeation barriers on polymers, Appl. Phys. Lett. 89 (2006) 081915, http://dx.doi.org/10.1063/1.2338776.
[15] M.D. Groner, S.M. George, R.S. McLean, P.F. Carcia, Gas diffusion barriers on polymers using Al_2O_3 atomic layer deposition, Appl. Phys. Lett. 88 (2006) 051907, http://dx.doi.org/10.10663/1.2168489.
[16] P.F. Carcia, R.S. McLean, M.H. Reilly, Permeation measurements and modeling of highly defective Al_2O_3 thin films grown by atomic layer deposition on polymers, Appl. Phys. Lett. 97 (2010) 221901, http://dx.doi.org/10.1063/1.3519476.
[17] P.F. Carcia, R.S. McLean, Z.G. Li, M.H. Reilly, W.J. Marshall, Permeability and corrosion in ZrO_2/Al_2O_3 nanolaminate and Al_2O_3 thin films grown by atomic layer deposition on polymers, J. Vac. Sci. Technol., A 30 (2012) 041515, http://dx.doi.org/10.1116/1.4729447.
[18] A. Singh, H. Klumbies, U. Schröder, L. Müller-Meskamp, M. Geidel, M. Knaut, et al., Barrier performance optimization of atomic layer deposited diffusion barriers for organic light emitting diodes using X-ray reflectivity investigations, Appl. Phys. Lett. 103 (2013) 233302, http://dx.doi.org/10.1063/1.4839455.
[19] R. Paetzold, A. Winnacker, D. Henseler, V. Cesari, K. Heuser, Permeation rate measurements by electrical analysis of calcium corrosion, Rev. Sci. Instrum. 74 (2003) 5147, http://dx.doi.org/10.1063/1.1626015.
[20] S. Schubert, H. Klumbies, L. Müller-Meskamp, K. Leo, Electrical calcium test for moisture barrier evaluation for organic devices, Rev. Sci. Instrum. 82 (2011) 094101, http://dx.doi.org/10.1063/1.3633956.
[21] H. Klumbies, L. Müller-Meskamp, T. Mönch, S. Schubert, K. Leo, The influence of laterally inhomogeneous corrosion on electrical and optical calcium moisture barrier characterization, Rev. Sci. Instrum. 84 (2013) 024103, http://dx.doi.org/10.1063/1.4791798.
[22] R. Meerheim, K. Walzer, M. Pfeiffer, K. Leo, Ultrastable and efficient red organic light emitting diodes with doped transport layers, Appl. Phys. Lett. 89 (2006) 061111, http://dx.doi.org/10.1063/1.2268354.
[23] M. Hermenau, S. Schubert, H. Klumbies, J. Fahlteich, L. Müller-Meskamp, K. Leo, et al., The effect of barrier performance on the lifetime of small-molecule organic solar cells, Sol. Energy Mater. Sol. Cells 97 (2012) 102–108, http://dx.doi.org/10.1016/j.solmat.2011.09.026.
[24] R. Paetzold, High-sensitivity permeation measurements on flexible OLED substrates, Proc. SPIE 5214 (2004) 73–82, http://dx.doi.org/10.1117/12.510027.
[25] H. Klumbies, L. Müller-Meskamp, F. Nehm, K. Leo, Note: influence of calcium corrosion on the performance of an adjacent permeation barrier, Rev. Sci. Instrum. 85 (2013) 016104, http://dx.doi.org/10.1063/1.4861536.
[26] E. Lakomaa, A. Root, T. Suntola, Surface reactions in Al_2O_3 growth from trimethylaluminum and water by atomic layer epitaxy, Appl. Surf. Sci. 107 (1996) 107–115, http://dx.doi.org/10.1016/S0169-4332(96)00513-2.